

Reevaluating R-parity Violating Supersymmetry Effects in $B_s^0 - \bar{B}_s^0$ Mixing

Ru-Min Wang*, Yuan-Guo Xu†, Mo-Lin Liu‡, Bing-Zhong Li§

College of Physics and Electronic Engineering, Xinyang Normal University, Xinyang, Henan 464000, China

September 28, 2018

Abstract

Recently, the CDF and DØ collaborations have claimed that the CP violating phase in $B_s^0 - \bar{B}_s^0$ mixing is large, which is contrary to the expectations in the Standard Model. Such a large phase suggests New Physics contributions to $B_s^0 - \bar{B}_s^0$ mixing. Motivated by this, we reevaluate the constraints on R-parity violating contributions, including baryon number violating couplings not considered before, to the mixing mass matrix element M_{12}^s from the recent measurements of $B_s^0 - \bar{B}_s^0$ mixing. We show that present data allow us to put quite strong constraints on both the magnitudes and the weak phases of the R-parity violating parameters. Some of these bounds are better than the existing ones, and some bounds are obtained for the first time. Near future experiments at the Tevatron, the LHC and B-factories can shrink or reveal the relevant parameter spaces of the R-parity violating couplings.

Keywords: B Physics, Neutral meson mixing, Supersymmetry, R-parity violating

PACS Numbers: 12.60.Jv, 11.30.Er, 12.15.Mm, 14.40.Nd

*E-mail: ruminwang@gmail.com

†E-mail: yuangx@iopp.cnu.edu.cn

‡E-mail: mliu@mail2.xyt.cnu.edu.cn

§E-mail: libingzhong08@yahoo.cn

1 Introduction

Mixing phenomena in heavy bosons system is considered as an important test of the Standard Model (SM) and a probe for New Physics (NP) beyond the SM. Recently, the large CP violating phase $\phi_s^{J/\psi\phi}$ associated with $B_s^0 - \bar{B}_s^0$ mixing has been obtained from the time-dependent angular analysis of flavor-tagged $B_s^0 \rightarrow J/\psi\phi$ decay by the CDF and DØ collaborations [1–3]. More recently, the DØ collaboration has announced evidence for a charge asymmetry in the number of like-sign dimuon events [4], which can be interpreted as further evidence for large CP violation in $B_s^0 - \bar{B}_s^0$ mixing. The CP violating phase measured by both CDF and DØ is [5]

$$\begin{aligned}\phi_s^{J/\psi\phi} &\in [0.54, 1.18] \cup [1.94, 2.60] \text{ (at 68\% C.L.)}, \\ \phi_s^{J/\psi\phi} &\in [0.20, 2.84] \text{ (at 95\% C.L.)}.\end{aligned}\tag{1}$$

However, the CP violating phase is predicted precisely to be small in the SM [6–10], $\phi_s^{J/\psi\phi, \text{SM}} = 2\beta_s^{\text{SM}} \equiv 2\arg\left(-\frac{V_{ts}V_{tb}^*}{V_{cs}V_{cb}^*}\right) \approx 0.04$. Current experimental data of the CP violating phase deviate about 2σ from its SM value, which indicates that there are possible large NP contributions to the phase, i.e., $\phi_s^{J/\psi\phi} = \phi_s^{J/\psi\phi, \text{SM}} + \phi_s^{\text{NP}}$.

In general, the relevant CP violating phase between the $B_s^0 - \bar{B}_s^0$ amplitude and the amplitudes of the subsequent B_s^0 and \bar{B}_s^0 decay to a common final state could be expressed as [11]

$$\phi_s = \arg\left(-\frac{M_{12}^s}{\Gamma_{12}^s}\right),\tag{2}$$

where M_{12}^s is the off-diagonal element of the $\Delta B = 2$ mass matrix, and Γ_{12}^s is the off-diagonal element of the decay matrix. The SM prediction for this phase is tiny, $\phi_s^{\text{SM}} \approx 0.004$ [7]. The same additional contribution ϕ_s^{NP} due to NP would change this observed phase, i.e., $\phi_s = \phi_s^{\text{SM}} + \phi_s^{\text{NP}}$.

The current experimental precision does not allow these small CP-violating phases $\phi_s^{J/\psi\phi, \text{SM}}$ and ϕ_s^{SM} to be resolved. In case of sizable NP contributions, the following approximation is used: $\phi_s^{J/\psi\phi} \approx \phi_s \approx \phi_s^{\text{NP}}$. In order to explain the large CP asymmetry, the NP contributions to M_{12}^s and Γ_{12}^s have already been widely studied in recent works (for example, see Refs. [12–19]).

As one of the most promising candidates for NP, Supersymmetry (SUSY) [20, 21], in both its R-parity conserving and its R-parity Violating (\mathcal{R}_p) incarnations, is extensively studied. In SUSY without R-parity, the following \mathcal{R}_p superpotential are also allowed [20]

$$\mathcal{W}_{\mathcal{R}_p} = \mu_i \hat{L}_i \hat{H}_u + \frac{1}{2} \lambda_{[ij]k} \hat{L}_i \hat{L}_j \hat{E}_k^c + \lambda'_{ijk} \hat{L}_i \hat{Q}_j \hat{D}_k^c + \frac{1}{2} \lambda''_{i[jk]} \hat{U}_i^c \hat{D}_j^c \hat{D}_k^c,\tag{3}$$

where the first three terms violate lepton number, and the last term violates baryon number. R_p SUSY effects in neutral meson mixing have been extensively discussed in the literatures (for example, Refs. [22–27]). In this paper, we focus on the lepton number violating (\mathcal{L}) and baryon number violating (\mathcal{B}) contributions to M_{12}^s in SUSY model without R-parity. Using the latest experimental data of $B_s^0 - \bar{B}_s^0$ mixing, we systematically evaluate the constraints on relevant \mathcal{L} and \mathcal{B} couplings. We improve the bounds on relevant \mathcal{L} couplings from current relevant data of $B_s^0 - \bar{B}_s^0$ mixing. We explore the \mathcal{B} coupling effects in $B_s^0 - \bar{B}_s^0$ mixing for the first time. We find our bounds on some \mathcal{B} coupling products from $B_s^0 - \bar{B}_s^0$ mixing are better than ones from relevant decays. Moreover, the bounds on some \mathcal{B} coupling products are derived for the first time.

This paper is organized as follows. We briefly review the theoretical basis for $B_s^0 - \bar{B}_s^0$ mixing in Section 2, then we deal with the numerical results in Section 3. In Section 4, we summarize and conclude.

2 Theoretical input for $B_s^0 - \bar{B}_s^0$ mixing

The most general $\Delta B = \Delta S = 2$ process is described by the effective Hamiltonian [28]

$$\mathcal{H}_{eff}(\Delta B = \Delta S = 2) = \sum_{i=1}^5 C_i Q_i + \sum_{i=1}^3 \tilde{C}_i \tilde{Q}_i + h.c., \quad (4)$$

with

$$Q_1 = (\bar{s}\gamma^\mu P_L b)_1 (\bar{s}\gamma_\mu P_L b)_1, \quad (5)$$

$$Q_2 = (\bar{s}P_L b)_1 (\bar{s}P_L b)_1, \quad (6)$$

$$Q_3 = (\bar{s}P_L b)_8 (\bar{s}P_L b)_8, \quad (7)$$

$$Q_4 = (\bar{s}P_L b)_1 (\bar{s}P_R b)_1, \quad (8)$$

$$Q_5 = (\bar{s}P_L b)_8 (\bar{s}P_R b)_8, \quad (9)$$

where $P_{L(R)} = (1 - (+)\gamma_5)/2$ and the operators $\tilde{Q}_{1,2,3}$ are obtained from $Q_{1,2,3}$ by the exchange $L \leftrightarrow R$. The hadronic matrix elements, taking into account for renormalization effects, are defined as follows

$$\langle \bar{B}_s^0 | Q_1(\mu) | B_s^0 \rangle = \frac{2}{3} m_{B_s}^2 f_{B_s}^2 B_1^{(s)}(\mu), \quad (10)$$

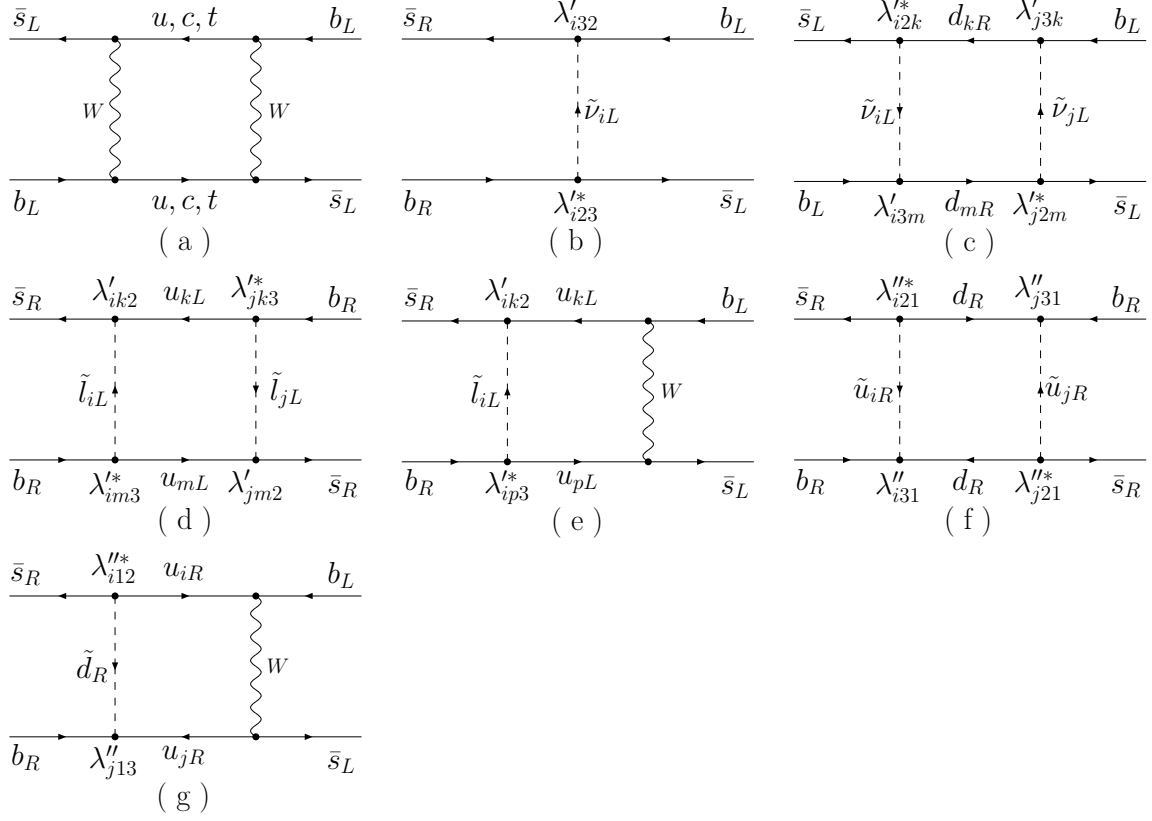


Figure 1: SM diagram (a), \mathcal{L} diagrams (b-e) and \mathcal{B} diagrams (f-g) which give the contributions to $B_s^0 - \bar{B}_s^0$ mixing.

$$\langle \bar{B}_s^0 | Q_2(\mu) | B_s^0 \rangle = -\frac{5}{12} m_{B_s}^2 f_{B_s}^2 S_{B_s} B_2^{(s)}(\mu), \quad (11)$$

$$\langle \bar{B}_s^0 | Q_3(\mu) | B_s^0 \rangle = \frac{1}{12} m_{B_s}^2 f_{B_s}^2 S_{B_s} B_3^{(s)}(\mu), \quad (12)$$

$$\langle \bar{B}_s^0 | Q_4(\mu) | B_s^0 \rangle = \frac{1}{2} m_{B_s}^2 f_{B_s}^2 S_{B_s} B_4^{(s)}(\mu), \quad (13)$$

$$\langle \bar{B}_s^0 | Q_5(\mu) | B_s^0 \rangle = \frac{1}{6} m_{B_s}^2 f_{B_s}^2 S_{B_s} B_5^{(s)}(\mu), \quad (14)$$

with $S_{B_s} = \left(\frac{m_{B_s}}{\bar{m}_b(m_b) + \bar{m}_s(m_b)} \right)^2$. The B -parameters given in Table 1 have been taken from Ref. [29].

The Wilson coefficients C_i receive contributions from both the SM and NP. In SUSY without R-parity, we only consider the \mathcal{R}_p NP effects for the Wilson coefficients, *i.e.*, $C_i \equiv C_i^{SM} + C_i^{\mathcal{R}_p}$. In the SM, the $t - W$ box diagram shown in Fig. 1(a) generates only contribution to the operator Q_1 , and the corresponding Wilson coefficient C_1^{SM} at the m_b scale is [30]

$$C_1^{SM}(m_b) = \frac{G_F^2}{4\pi^2} m_W^2 (V_{ts} V_{tb}^*)^2 \eta_{2B} S_0(x_t) [\alpha_s(m_b)]^{-6/23} \left[1 + \frac{\alpha_s(m_b)}{4\pi} J_5 \right], \quad (15)$$

where $x_t = m_t^2/m_W^2$ and η_{2B} is the QCD correction.

Now we turn to the \mathcal{R}_p SUSY contributions to $B_s^0 - \bar{B}_s^0$ mixing. In the most general superpotential of the minimal supersymmetric SM, there are new contributions to $B_s^0 - \bar{B}_s^0$ mixing from \mathcal{R}_p couplings, and the corresponding Wilson coefficients can be obtained from the \mathcal{R}_p superpotential given in Eq. (3)

$$\begin{aligned}
C_1^{\mathcal{R}_p} &= C_1^{\lambda'}, \\
C_4^{\mathcal{R}_p} &= C_4^{TL} + C_4^{\lambda'W} + C_4^{\lambda''W}, \\
C_5^{\mathcal{R}_p} &= C_5^{\lambda'} + C_5^{\lambda''W}, \\
\tilde{C}_1^{\mathcal{R}_p} &= \tilde{C}_1^{\lambda'} + \tilde{C}_1^{\lambda''}.
\end{aligned} \tag{16}$$

Contributions to Wilson coefficients in Eq. (16) come from a variety of different classes of \mathcal{R}_p diagrams, some of which are shown in Fig. 1. One must add the diagrams as shown in Fig. 1(c,d,f) by exchange of internal fermions \leftrightarrow corresponding internal sfermions. C_4^{TL} denotes the only tree level diagram with the exchange of a sneutrino $\tilde{\nu}_i$ and two λ' couplings, which is shown in Fig. 1(b). The λ' box diagrams such as Fig. 1(c) give a contribution to $C_1^{\lambda'}$, $\tilde{C}_1^{\lambda'}$ and $C_5^{\lambda'}$. The λ' box diagrams such as Fig. 1(d) only give a contribution to $\tilde{C}_1^{\lambda'}$. The $\lambda' - W$ box diagrams such as Fig. 1(e) with one internal W boson and one internal slepton give a contribution to $C_4^{\lambda'W}$. The λ'' box diagrams such as Fig. 1(f) give a contribution to $\tilde{C}_1^{\lambda''}$. As shown in Fig. 1(g), the $\lambda'' - W$ box diagram gives a contribution to both $C_4^{\lambda''W}$ and $C_5^{\lambda''W}$. The coefficients in Eq. (16) are given by [23, 26]

$$C_1^{\lambda'} = \frac{1}{64\pi^2} \sum_{i,j,k,m} \lambda'_{i2k} \lambda'_{j3k} \lambda'_{j2m} \lambda'_{i3m} \left[I_4(m_{\tilde{\nu}_i}^2, m_{\tilde{\nu}_j}^2, m_{d_k}^2, m_{d_m}^2) + I_4(m_{\nu_i}^2, m_{\nu_j}^2, m_{d_k^*}^2, m_{d_m^*}^2) \right], \tag{17}$$

$$\begin{aligned}
\tilde{C}_1^{\lambda'} &= \frac{1}{64\pi^2} \sum_{i,j,k,m} \lambda'_{ik2} \lambda'_{jk3} \lambda'_{jm2} \lambda'_{im3} \left[I_4(m_{\tilde{\nu}_i}^2, m_{\tilde{\nu}_j}^2, m_{d_k}^2, m_{d_m}^2) + I_4(m_{\nu_i}^2, m_{\nu_j}^2, m_{d_k^*}^2, m_{d_m^*}^2) \right. \\
&\quad \left. + I_4(m_{\tilde{e}_i}^2, m_{\tilde{e}_j}^2, m_{u_k}^2, m_{u_m}^2) + I_4(m_{e_i}^2, m_{e_j}^2, m_{u_k^*}^2, m_{u_m^*}^2) \right], \tag{18}
\end{aligned}$$

$$\tilde{C}_1^{\lambda''} = \frac{1}{32\pi^2} \sum_{i,j} \lambda''_{i21} \lambda''_{i31} \lambda''_{j21} \lambda''_{j31} \left[I_4(m_d^2, m_d^2, m_{\tilde{u}_R^i}^2, m_{\tilde{u}_R^j}^2) + I_4(m_{d_R}^2, m_{d_R}^2, m_{u_i}^2, m_{u_j}^2) \right], \tag{19}$$

$$C_4^{TL} = \sum_i \frac{\lambda'_{i32} \lambda'_{i23}}{m_{\tilde{\nu}_i}^2}, \tag{20}$$

$$C_4^{\lambda'W} = \frac{G_F}{4\sqrt{2}\pi^2} \lambda'_{ik2} \lambda'_{ip3} V_{u_p s}^* V_{u_k b} F(m_{u_k}^2/m_{\tilde{l}_i}^2), \tag{21}$$

$$C_4^{\lambda''W} = -\frac{\alpha}{4\pi \sin^2 \theta_W} \sum_{i,j} \lambda''_{i21} \lambda''_{j31} V_{u_i s}^* V_{u_j b} m_{u_i} m_{u_j} J_4(m_{d_R}^2, M_W^2, m_{u_i}^2, m_{u_j}^2), \tag{22}$$

$$C_5^{\lambda'} = -\frac{1}{32\pi^2} \sum_{i,j,k,m} \lambda'_{i2k} \lambda'_{j3k} \lambda'_{im2} \lambda'_{jm3} \left[I_4(m_{\tilde{\nu}_i}^2, m_{\tilde{\nu}_j}^2, m_{d_k}^2, m_{d_m}^2) + I_4(m_{\nu_i}^2, m_{\nu_j}^2, m_{d_k^*}^2, m_{d_m^*}^2) \right] \tag{23}$$

$$C_5^{\lambda''W} = \frac{\alpha}{4\pi \sin^2 \theta_W} \sum_{i,j} \lambda''_{i21} \lambda''_{j31} V_{u_i s}^* V_{u_j b} m_{u_i} m_{u_j} J_4(m_{d_R}^2, M_W^2, m_{u_i}^2, m_{u_j}^2), \tag{24}$$

where the functions $I_4(m_1^2, m_2^2, m_3^2, m_4^2)$ and $J_4(m_1^2, m_2^2, m_3^2, m_4^2)$ are defined in Ref. [26], $F(x)$ is $I(x)$ for $p = k$ as well as $L(x)$ for $p \neq k$, and the definitions of $I(x)$ and $L(x)$ can be found in Ref. [23].

In terms of the effective Hamiltonian given in Eq. (4), M_{12}^s reads

$$M_{12}^s = \frac{\langle B_s^0 | \mathcal{H}_{eff}(\Delta B = \Delta S = 2) | \bar{B}_s^0 \rangle}{2m_{B_s}}. \quad (25)$$

In the SM, the off-diagonal element of the decay matrix $\Gamma_{12}^{s,SM}$ may be written as [31]

$$\Gamma_{12}^{s,SM} = -\frac{G_F^2 m_b^2}{8\pi M_{B_s}} (V_{cs} V_{cb}^*)^2 \left[G(x_c) \langle B_s^0 | Q_1 | \bar{B}_s^0 \rangle + G_2(x_c) \langle B_s^0 | Q_2 | \bar{B}_s^0 \rangle + \sqrt{1 - 4x_c} \hat{\delta}_{1/m} \right], \quad (26)$$

where $x_c = m_c^2/m_b^2$, $G(x_c) = 0.030$ and $G_2(x_c) = -0.937$ at the m_b scale [31], and the $1/m_b$ corrections $\hat{\delta}_{1/m}$ are given in Ref. [32]. It's important to note that NP can significantly affect M_{12}^s , but not Γ_{12}^s , which is dominated by the CKM favored $b \rightarrow c\bar{c}s$ tree-level decays. Hence $\Gamma_{12}^s = \Gamma_{12}^{s,SM}$ holds as a good approximation [7, 33].

In this work, besides the CP violating phase $\phi_s^{J/\psi\phi}$, the experimental bounds of the following quantities will be considered.

- The B_s mass difference: $\Delta M_s = 2 |M_{12}^s|$.
- The B_s width difference [34]: $\Delta\Gamma_s = \frac{4|Re(M_{12}^s \Gamma_{12}^{s*})|}{\Delta M_s} \approx 2|\Gamma_{12}^s| \cos\phi_s$.
- The semileptonic CP asymmetry in B_s decays [35, 36]: $A_{SL}^s = \text{Im}\left(\frac{\Gamma_{12}^s}{M_{12}^s}\right) = \frac{\Delta\Gamma_s}{\Delta M_s} \tan\phi_s$.

3 Numerical results and discussions

In this section, we summarize our numerical results and analysis of \mathcal{L} as well as \mathcal{B} coupling effects in $B_s^0 - \bar{B}_s^0$ mixing. The theoretical input parameters used in our work are collected in Table 1. In our numerical results, we use the theoretical input parameters and the experimental constraints at 95% C.L.. For the general case, we consider the \mathcal{R}_p coupling constants are complex, the phases of the \mathcal{R}_p coupling products are varied from $-\pi$ to π , while the moduli of the coupling products are assumed to be only positive. When we study the \mathcal{R}_p effects, we consider only one kind of the \mathcal{R}_p coupling contributions at one time, neglecting the interferences between different kinds of the \mathcal{R}_p coupling products, but keeping their interferences with the SM contributions. In addition, we assume the masses of sfermions are 500 GeV.

Table 1: Values of the theoretical input parameters. To be conservative, we use all theoretical input parameters at 95% C.L. in our numerical results. The B_i^s parameters are taken from Ref. [29] in the RI/MOM scheme, where the first error is the statistical one and the second error is the systematic one.

$m_W = 80.398 \pm 0.025 \text{ GeV}, \quad m_{B_s} = 5.3663 \pm 0.0006 \text{ GeV},$	
$\overline{m}_b(\overline{m}_b) = 4.20_{-0.07}^{+0.17} \text{ GeV}, \quad \overline{m}_s(2\text{GeV}) = 0.105_{-0.035}^{+0.025} \text{ GeV},$	
$m_t = 171.3_{-1.6}^{+2.1} \text{ GeV}, \quad m_b = 4.85 \pm 0.15 \text{ GeV}.$	[37]
$A = 0.810 \pm 0.013, \quad \lambda = 0.2259 \pm 0.0016, \quad \bar{\rho} = 0.177 \pm 0.044, \quad \bar{\eta} = 0.360 \pm 0.031.$	[38]
$\eta_{2B} = 0.55 \pm 0.01.$	[39]
$f_{B_s} = 0.230 \pm 0.030 \text{ GeV}.$	[40]
$B_1^{(s)}(m_b) = 0.86(2) \binom{+5}{-4}, \quad B_2^{(s)}(m_b) = 0.83(2)(4), \quad B_3^{(s)}(m_b) = 1.03(4)(9),$	
$B_4^{(s)}(m_b) = 1.17(2) \binom{+5}{-7}, \quad B_5^{(s)}(m_b) = 1.94(3) \binom{+23}{-7}.$	[29]

The following experimental data at 95% C.L. are used to constrain relevant R_p couplings [1, 2, 4, 5]

$$\phi_s^{J/\psi\phi} \in [0.20, 2.84] \text{ (at 95\% C.L.)}, \quad (27)$$

$$\Delta M_s = 17.77 \pm 0.12, \quad (28)$$

$$\Delta \Gamma_s = 0.19 \pm 0.07, \quad (29)$$

$$A_{SL}^s = (1.46 \pm 0.75) \times 10^{-2}. \quad (30)$$

3.1 \mathcal{L} couplings

Now we discuss the constraints on the \mathcal{L} coupling spaces. By using the experimental data and the theoretical input parameters at 95% C.L., which are given in Eqs. (27-30) and Table 1, respectively, we constrain the allowed ranges of relevant \mathcal{L} couplings.

First of all, we take $\lambda'_{i32}\lambda_{i33}^*$ couplings, which arise from the $\lambda' - W$ box diagram such as Fig. 1(e), as an example to illuminate the bounds from different observables in Eqs. (27-30). Fig. 2 displays the allowed spaces for $\lambda'_{i32}\lambda_{i33}^*$ constrained by the experimental data of $\phi_s^{J/\psi\phi}$, ΔM_s , $\Delta \Gamma_s$ and A_{SL}^s . In Fig. 2, we only show the regions of $|\lambda'_{i32}\lambda_{i33}^*|$ belongs to $[0, 3.5 \times 10^{-2}]$, and the regions of $|\lambda'_{i32}\lambda_{i33}^*| > 3.5 \times 10^{-2}$ is still allowed for the bounds from $\phi_s^{J/\psi\phi}$, $\Delta \Gamma_s$ and

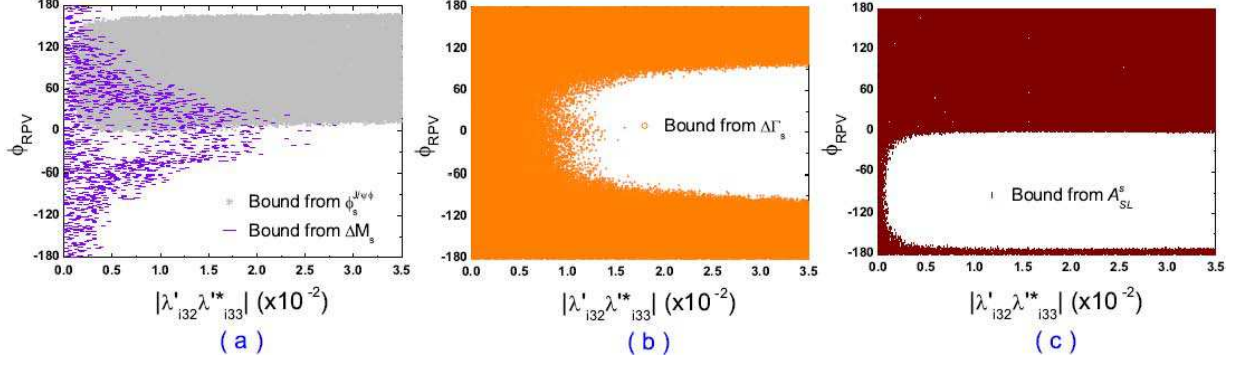


Figure 2: Allowed parameter space for $\lambda'_{i32}\lambda^*_{i33}$ constrained by $\phi_s^{J/\psi\phi}$ (light gray), ΔM_s (violet), $\Delta\Gamma_s$ (orange) and A_{SL}^s (wine), respectively. The \mathcal{R}_p weak phases ϕ_{RPV} are given in degree.

A_{SL}^s . The light gray region in Fig. 2 (a) shows the constrained space from $\phi_s^{J/\psi\phi}$, and we can see that current data of $\phi_s^{J/\psi\phi}$ at 95% C.L. give quite strong constraint on the \mathcal{R}_p weak phases of $\lambda'_{i32}\lambda^*_{i33}$. Moreover, the lower limits of $|\lambda'_{i32}\lambda^*_{i33}|$ are also constrained by $\phi_s^{J/\psi\phi}$ since its data at 95% C.L. are not consistent with its SM value. The violet region in Fig. 2 (a) displays the constrained space from ΔM_s , and we see that current data of ΔM_s at 95% C.L. could obviously constrain the \mathcal{R}_p weak phases as well as the upper limits of $|\lambda'_{i32}\lambda^*_{i33}|$. The orange region in Fig. 2 (b) is the constrained space from $\Delta\Gamma_s$, and we see that $\Delta\Gamma_s$ gives the bound on the \mathcal{R}_p weak phases when $|\lambda'_{i32}\lambda^*_{i33}| > 1.4 \times 10^{-2}$. The wine region in Fig. 2 (c) shows the constrained space from A_{SL}^s , and we see that whole region for $\phi_{RPV} > 0$ and some region for $\phi_{RPV} < 0$ are allowed. We find that the bound from A_{SL}^s displayed in Fig. 2 (c) is weaker than one from $\phi_s^{J/\psi\phi}$ displayed in Fig. 2 (a), therefore A_{SL}^s does not give any useful constraint if we consider all experimental data given in Eq. (30) to constrain $\lambda'_{i32}\lambda^*_{i33}$ couplings. From Fig. 2, we know that, if we consider the experimental bounds of $\phi_s^{J/\psi\phi}$, ΔM_s and $\Delta\Gamma_s$ at the same time, the upper limits of $|\lambda'_{i32}\lambda^*_{i33}|$ are constrained by ΔM_s and $\Delta\Gamma_s$, the lower limits of $|\lambda'_{i32}\lambda^*_{i33}|$ are constrained by $\phi_s^{J/\psi\phi}$, both upper and lower limits of the \mathcal{R}_p weak phase are constrained by ΔM_s and $\phi_s^{J/\psi\phi}$.

Next, using the experimental data in Eqs.(27-30), we give the constrained spaces of relevant \mathcal{L} couplings. Fig. 3 shows the allowed spaces which arise from the $\lambda' - W$ box diagram as displayed in Fig. 1(e). Other constrained parameter spaces of \mathcal{L} couplings have not been on show, since their allowed \mathcal{R}_p weak phases have similar allowed regions to one of the plots in Fig. 3. From Fig. 3, we see that current experimental data of $\phi_s^{J/\psi\phi}$ and ΔM_s give very strong bounds on both moduli and phases of all relevant \mathcal{L} coupling products, and the upper limits

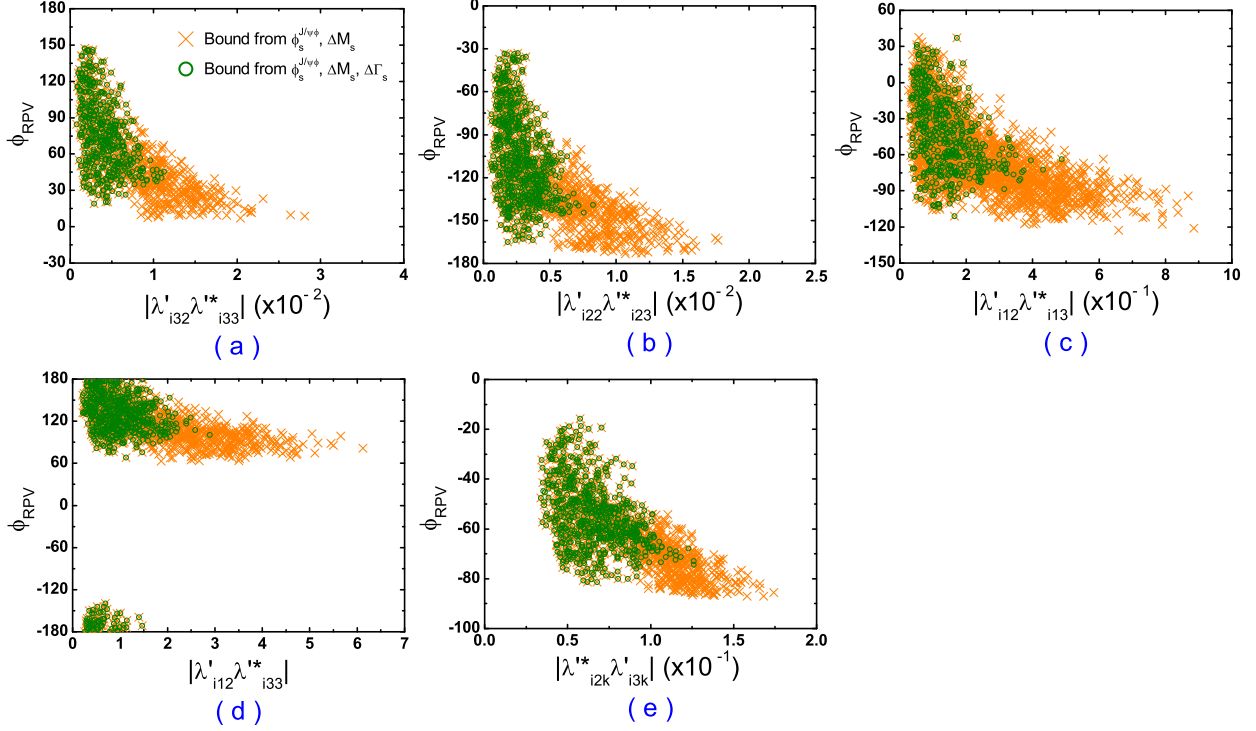


Figure 3: The constrained parameter spaces for some relevant \mathcal{L} couplings.

of moduli of all \mathcal{L} coupling products are further restricted by $\Delta\Gamma_s$.

Now we describe the correlation of the \mathcal{L} coupling phases as follows. The \mathcal{L} couplings $\lambda'_{i22}\lambda'^*_{i33}$, which arise from the $\lambda' - W$ box diagram, have similar allowed phases as shown in Fig. 3(a). The couplings $\lambda'^*_{i2k}\lambda'_{i3k}\lambda'_{ik2}\lambda'^*_{ik3}$, which are from the λ' box diagrams such as Fig. 1(c), also have similar allowed phases as shown in Fig. 3(a). $\lambda'_{i32}\lambda'^*_{i23}$ from tree-level diagram shown in Fig. 1(b) have similar allowed regions of \mathcal{R}_p phases to the region in Fig. 3(b). $\lambda'_{i22}\lambda'^*_{i13}$, $\lambda'_{i32}\lambda'^*_{i13}$ and $\lambda'_{i32}\lambda'^*_{i23}$ from the $\lambda' - W$ box diagram also have similar phase regions to one in Fig. 3(b). The phases of $\lambda'_{i12}\lambda'^*_{i23}$ constrained from the $\lambda' - W$ box diagram have similar region to Fig. 3(c). $\lambda'_{im2}\lambda'^*_{im3}$ ($m = 1, 2, 3$) and $\lambda'^*_{i2k}\lambda'_{i3k}$ ($k = 1, 2, 3$) are from the λ' box diagrams such as Fig. 1(c-d), and the constrained phases of $\lambda'_{im2}\lambda'^*_{im3}$ ($m = 1, 2, 3$) have similar allowed regions to the constrained phases of $\lambda'^*_{i2k}\lambda'_{i3k}$ displayed in Fig. 3(e).

The relevant numerical bounds on moduli of \mathcal{L} coupling products are summarized in Table 2. Previous bounds are also listed for comparison. We present some remarks on the moduli of all relevant \mathcal{L} coupling products:

- Almost all bounds on the moduli of \mathcal{L} coupling products from current 95% C.L. data of ΔM_s , $\phi_s^{J/\psi\phi}$ and $\Delta\Gamma_s$ are stronger than previous ones in Refs. [22, 41], which are obtained only from the 68% C.L. data of ΔM_s . \mathcal{L} couplings that may contribute to $B_s^0 - \bar{B}_s^0$ mixing

Table 2: Bounds on moduli of the relevant \mathcal{L} coupling products for 500 GeV sfermions, and previous bounds are listed for comparison. The allowed ranges within the square brackets are obtained from the experimental constraints given in Eqs. (27-30) and the theoretical input parameters listed in Table 1 at 95% C.L.. “ b ” denotes that the couplings are constrained from the λ' box diagrams such as Fig. 1(c-d), “ b' ” denotes that the couplings are constrained from the $\lambda' - W$ box diagram as Fig. 1(e), and “ t ” denotes that the couplings are bounded from the tree level diagram as Fig. 1(b). (The similar signs are used in Table 3).

Line No.	Couplings	From $\phi_s^{J/\psi\phi}, \Delta M_s$	From $\phi_s^{J/\psi\phi}, \Delta M_s, \Delta\Gamma_s$	Previous Bounds
1	$ \lambda'_{i32}\lambda_{i33}^* (\times 10^{-1})^b$	[0.30, 1.91]	[0.30, 1.39]	< 8.75 [26]
2	$ \lambda'_{i32}\lambda_{i33}^* (\times 10^{-2})^{b'}$	[0.08, 2.81]	[0.08, 1.13]	< 3.9 [22]
3	$ \lambda'_{i22}\lambda_{i23}^* (\times 10^{-1})^b$	[0.29, 1.74]	[0.29, 1.26]	< 8.75 [26]
4	$ \lambda'_{i22}\lambda_{i23}^* (\times 10^{-2})^{b'}$	[0.06, 1.87]	[0.06, 1.06]	< 3.1 [22]
5	$ \lambda'_{i12}\lambda_{i13}^* (\times 10^{-1})^b$	[0.29, 1.74]	[0.29, 1.26]	< 8.75 [26]
6	$ \lambda'_{i12}\lambda_{i13}^* (\times 10^{-1})^{b'}$	[0.26, 8.85]	[0.26, 4.88]	< 1.45 [22]
7	$ \lambda'_{i32}\lambda_{i23}^* (\times 10^{-5})^t$	[0.13, 4.07]	[0.13, 1.84]	< 3.5 [41]
8	$ \lambda'_{i32}\lambda_{i23}^* (\times 10^{-4})^{b'}$	[0.28, 9.13]	[0.28, 4.57]	< 10.5 [22]
9	$ \lambda'_{i22}\lambda_{i33}^* (\times 10^{-1})^{b'}$	[0.15, 5.22]	[0.15, 2.71]	< 5.9 [22]
10	$ \lambda'_{i22}\lambda_{i13}^* (\times 10^{-2})^{b'}$	[0.24, 7.87]	[0.24, 3.65]	< 4.9 [22]
11	$ \lambda'_{i12}\lambda_{i23}^* (\times 10^{-1})^{b'}$	[0.07, 2.29]	[0.07, 1.38]	< 1.0 [22]
12	$ \lambda'_{i32}\lambda_{i13}^* (\times 10^{-3})^{b'}$	[0.13, 4.10]	[0.13, 1.80]	< 4.6 [22]
13	$ \lambda'_{i12}\lambda_{i33}^* ^{b'}$	[0.21, 6.13]	[0.21, 2.89]	< 3.1 [22]
14	$ \lambda'_{i23}\lambda_{i33}^* (\times 10^{-1})^b$	[0.29, 1.74]	[0.29, 1.26]	< 2.0 [22, 26]
15	$ \lambda'_{i22}\lambda_{i32}^* (\times 10^{-1})^b$	[0.29, 1.74]	[0.29, 1.26]	< 2.0 [22, 26]
16	$ \lambda'_{i21}\lambda_{i31}^* (\times 10^{-1})^b$	[0.29, 1.74]	[0.29, 1.26]	< 2.0 [22, 26]
17	$ \lambda_{i2k}^*\lambda'_{i3k}\lambda'_{ik2}\lambda_{ik3}^* (\times 10^{-2})^b$	[0.06, 2.43]	[0.06, 1.23]	

also affect various decays, relevant \mathcal{L} coupling effects in the decays have already been studied in Refs. [22, 26, 42, 43], and some moduli of them may have better bounds from the decays.

- $\lambda'_{ik2}\lambda_{ik3}^*$ ($k = 1, 2, 3$) couplings arise in both the λ' box diagrams and the $\lambda' - W$ box

diagram. In this work, we only consider one kind of diagrams at once. For $|\lambda'_{ik2}\lambda'^*_{ik3}|$ ($k = 2, 3$), as listed in the first four lines of Table 2, the contributions of these couplings to the λ' box diagrams are smaller than ones to the $\lambda' - W$ box diagram, and there are more than one order difference between two kinds of diagrams. Therefore, the stronger bounds on $|\lambda'_{ik2}\lambda'^*_{ik3}|$ ($k = 2, 3$) are constrained from the $\lambda' - W$ box diagram. If we consider these two kinds of diagrams at the same time, the bounds on $|\lambda'_{ik2}\lambda'^*_{ik3}|$ ($k = 2, 3$) are closed to ones only from the $\lambda' - W$ diagram. For $|\lambda'_{i12}\lambda'^*_{i13}|$, the contributions from the λ' box diagrams are sensitive to sfermion masses, but the contributions from the $\lambda' - W$ box diagram are not sensitive to sfermion masses. For 500 GeV sfermion masses, the couplings raised in both the λ' box diagrams and the $\lambda' - W$ box diagram give similar contributions.

- The contributions of $\lambda'_{ik2}\lambda'^*_{ik3}$ from the $\lambda' - W$ box diagram are proportional to the CKM matrix elements $V_{uks}^*V_{ukb}$ and the function $I(m_{u_k}^2/m_{\tilde{l}_i}^2)$. The bound differences between $|\lambda'_{i32}\lambda'^*_{i33}|$ and $|\lambda'_{ik2}\lambda'^*_{ik3}|$ ($k = 1, 2$) come from the CKM matrix elements and internal quark mass m_{u_k} . The bound differences between $|\lambda'_{i12}\lambda'^*_{i13}|$ and $|\lambda'_{i22}\lambda'^*_{i23}|$ mainly come from the CKM matrix elements since $I(m_c^2/m_{\tilde{l}_i}^2) \approx I(m_u^2/m_{\tilde{l}_i}^2)$. For this reason, as listed in Lines 4 and 6 of Table 2, $|\lambda'_{i12}\lambda'^*_{i13}|/|\lambda'_{i22}\lambda'^*_{i23}| \approx |V_{cs}^*V_{cb}|/|V_{us}^*V_{ub}| \approx 46$.
- $\lambda'_{i32}\lambda'^*_{i23}$ couplings arise in both the tree level diagram and the $\lambda' - W$ box diagram. Compared bounds listed in Lines 7-8 of Table 2, we can see that the stronger bounds on $|\lambda'_{i32}\lambda'^*_{i23}|$ come from the tree level contributions.
- $\lambda'_{ik2}\lambda'^*_{ip3}$ ($k \neq p$) couplings arise in the $\lambda' - W$ box diagram. As given in Eq. (21), their contributions are proportional to the corresponding CKM matrix elements $V_{ups}^*V_{ukb}$ and the function $F(m_{u_k}^2/m_{\tilde{l}_i}^2)$. Their bounds are listed in Lines 8-13 of Table 2, and the bound differences between $|\lambda'_{ik2}\lambda'^*_{ip3}|$ and $|\lambda'_{ip2}\lambda'^*_{ik3}|$ are due to the different CKM matrix elements.

3.2 \mathcal{B} couplings

Now we turn to discuss \mathcal{B} couplings. As given in Eqs. (22-24), \mathcal{B} couplings $\lambda''_{i21}\lambda''^*_{j31}$ ($i, j = 1, 2, 3$) from the $\lambda'' - W$ box diagram such as Fig. 1(g) are suppressed by the CKM matrix elements $V_{uis}^*V_{ujb}$ and the quark masses $m_{u_i}m_{u_j}$. Therefore, we don't consider the \mathcal{B} couplings of $\lambda''_{i21}\lambda''^*_{j31}$ (i or $j = 1$) in this work since they are significantly suppressed by m_u , V_{us} and V_{ub} .

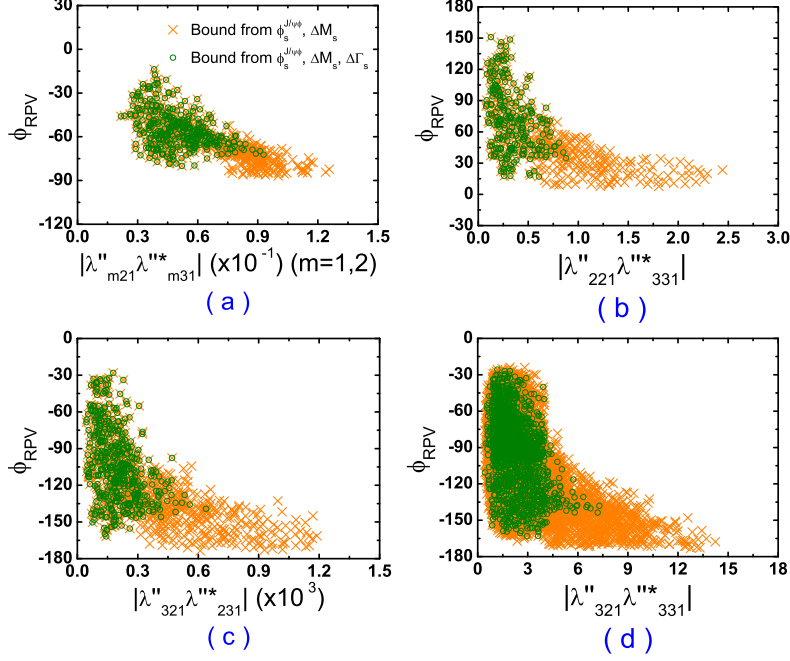


Figure 4: The constrained parameter spaces for some relevant \mathcal{B} couplings.

We can see later the bounds on moduli of $\lambda''_{i21}\lambda''_{j31}$ ($i, j \neq 1$) couplings from the $\lambda'' - W$ box diagram of Fig. 1(g) are very weak for this reason.

In Fig. 4, we show some constrained parameter spaces of \mathcal{B} couplings from the experimental data given in Eqs. (27-30). Fig. 4(a) displays the constrained spaces of $\lambda''_{m21}\lambda''_{m31}$ ($m = 1, 2$) couplings, which are from the λ'' box diagrams such as Fig. 1(f). The constrained spaces of $\lambda''_{221}\lambda''_{331}$, $\lambda''_{321}\lambda''_{231}$ and $\lambda''_{321}\lambda''_{331}$, which present in the $\lambda'' - W$ box diagram as Fig. 1(g), are displayed in Fig. 4(b-d). Other two relevant couplings $\lambda''_{321}\lambda''_{331}$ and $\lambda''_{221}\lambda''_{231}$, which arise in the λ'' box diagrams, have not been shown in Fig. 4. The allowed phase of $\lambda''_{321}\lambda''_{331}$ is similar to one in Fig. 4(a), and the allowed phase of $\lambda''_{221}\lambda''_{231}$ is similar to one in Fig. 4(b). We can see that current 95% C.L. experimental data of $B_s^0 - \bar{B}_s^0$ mixing give very strong bounds on relevant \mathcal{B} phases. However, they do not constrain some moduli a lot.

Our bounds on the moduli of relevant \mathcal{B} coupling products are listed in Table 3. Table 3 shows us that the upper limits of all relevant moduli of \mathcal{B} coupling products are further restricted by $\Delta\Gamma_s$. From the first six lines of this table, we easily see that the λ'' box diagrams give the dominant contributions to $B_s^0 - \bar{B}_s^0$ mixing. The bounds on $|\lambda''_{i21}\lambda''_{i31}|$ from the λ'' box diagrams are much stronger than ones from the $\lambda'' - W$ box diagram, since the contributions of the $\lambda'' - W$ box diagram are suppressed by internal up-type quark masses and relevant CKM

Table 3: Bounds on moduli of the relevant \mathcal{B} coupling products for 500 GeV sfermions. The allowed ranges within the square brackets are obtained from the experimental data given in Eqs. (27-30) and the theoretical input parameters listed in Table 1 at 95% C.L..

Line No.	Couplings	From $\phi_s^{J/\psi\phi}, \Delta M_s$	From $\phi_s^{J/\psi\phi}, \Delta M_s, \Delta\Gamma_s$
1	$ \lambda''_{321}\lambda''_{331} (\times 10^{-1})^b$	[0.22, 1.41]	[0.22, 0.96]
2	$ \lambda''_{321}\lambda''_{331} (\times 10^{-1})^{b'}$	[0.43, 14.23]	[0.43, 7.29]
3	$ \lambda''_{221}\lambda''_{231} (\times 10^{-1})^b$	[0.19, 1.26]	[0.19, 0.93]
4	$ \lambda''_{221}\lambda''_{231} (\times 10^2)^{b'}$	[0.10, 3.47]	[0.10, 1.66]
5	$ \lambda''_{121}\lambda''_{131} (\times 10^{-1})^b$	[0.19, 1.26]	[0.19, 0.93]
6	$ \lambda''_{321}\lambda''_{231} (\times 10^3)^{b'}$	[0.04, 1.19]	[0.04, 0.64]
7	$ \lambda''_{221}\lambda''_{331} ^{b'}$	[0.07, 2.44]	[0.07, 0.92]

matrix elements. Therefore, if we consider the contributions from the λ'' box diagrams and the $\lambda'' - W$ box diagram at the same time, the bound on $|\lambda''_{i21}\lambda''_{i31}|$ is close to the constraint only from the λ'' box diagrams. As listed in the last line of Table 3, $|\lambda''_{321}\lambda''_{231}|$ has very weak constraints from current data, since the $\lambda''_{321}\lambda''_{231}$ contributions are suppressed by m_c and $V_{ts}V_{cb}$.

The relevant bounds of the \mathcal{B} coupling products have already been obtained in Refs. [26, 42, 44, 45], and we summarize them with 500 GeV sfermion mass as follows.

- $|\lambda''_{i21}\lambda''_{i31}| < 1.0 \times 10^{-1}$ from $B^+ \rightarrow \bar{K}^0\pi^+$ decay [44].
- $|\lambda''_{i21}\lambda''_{i31}| < 1.54 \times 10^{-1}$ from $\frac{\Gamma(B^+ \rightarrow \bar{K}^0\pi^+)}{\Gamma(B^+ \rightarrow J/\psi K^+)}$ [26].
- $|\lambda''_{i21}\lambda''_{i31}| \in [9.3 \times 10^{-3}, 1.2 \times 10^{-1}] \cup [3.4 \times 10^{-1}, 4.0 \times 10^{-1}]$ from $B^+ \rightarrow \bar{K}^0\pi^+, K^+\pi^0$ [42].
- $|\lambda''_{i2k}\lambda''_{i3k}| < 4$ from $B \rightarrow K^*\gamma$ decays [44].
- $|\lambda''_{32k}\lambda''_{33k}| < 8.75$ from $\mathcal{B}(B \rightarrow X_s\gamma)$ [45].

Comparing our results with the existing ones listed above, our upper limits of $|\lambda''_{i21}\lambda''_{i31}|$ ($i = 1, 2, 3$) from the λ'' box diagrams listed in Lines 1,3,5 of Table 3 are a little stronger than the existing ones. In addition, the lower limits are also obtained from $B_s^0 - \bar{B}_s^0$ mixing since some relevant data are not consistent with the SM predictions at 95% C.L. As for $\lambda''_{321}\lambda''_{231}$ and $\lambda''_{221}\lambda''_{331}$ coupling products, their bounds are derived for the first time in this work.

4 Summary

The flavor changing processes in the $b - s$ sector are sensitive to probing of NP beyond the SM because they have the least constraint in current experiment aspect. Recent measurements of the CP violating phase by the $D\bar{O}$ and CDF collaborations exclude the SM predictions at 95% C.L., and this suggests NP beyond the SM contributing to $B_s^0 - \bar{B}_s^0$ mixing. Motivated by this, we have analyzed the constraints imposed on the parameter space of \mathcal{L} and \mathcal{B} contributions to M_{12}^s in \mathcal{R}_p SUSY. We have shown that current experimental data in $B_s^0 - \bar{B}_s^0$ mixing can be explained by the \mathcal{R}_p SUSY effects. Current data of ΔM_s , $\phi_s^{J/\psi\phi}$ and $\Delta\Gamma_s$ give quite strong bounds on some moduli and phases of relevant couplings. And the data of A_{SL}^s doesn't give any useful constraint since the bounds from A_{SL}^s are weaker than ones from $\phi_s^{J/\psi\phi}$.

We first considered \mathcal{L} coupling effects in $B_s^0 - \bar{B}_s^0$ mixing. The similar analysis was performed only from the bound on ΔM_s in Refs. [22, 41], in this paper we have used the current bounds not only on ΔM_s but also on $\phi_s^{J/\psi\phi}$ and $\Delta\Gamma_s$ as given in Eqs. (27-30). We have found that almost all bounds on the moduli of \mathcal{L} coupling products from current 95% C.L. data of ΔM_s , $\phi_s^{J/\psi\phi}$ and $\Delta\Gamma_s$ are much stronger than previous ones only from the 68% C.L. data of ΔM_s [22, 41]. We also have obtained quite strong bounds on the \mathcal{R}_p weak phases of these coupling products. Noted that some \mathcal{L} couplings, which may contribute to $B_s^0 - \bar{B}_s^0$ mixing, also affect various decays, and the moduli of these \mathcal{L} couplings may still have better bounds from relevant decays.

For \mathcal{B} coupling effects in $B_s^0 - \bar{B}_s^0$ mixing, we studied them for the first time in this work. We have found that our bounds on the moduli of $\lambda''_{i21}\lambda''_{i31}^*$ ($i = 1, 2, 3$) from current data of $B_s^0 - \bar{B}_s^0$ mixing are stronger than ones from relevant decays. And we have obtained very strong bounds on the \mathcal{R}_p weak phases of $\lambda''_{i21}\lambda''_{i31}^*$ ($i = 1, 2, 3$). In addition, the bounds on the \mathcal{B} coupling products, $\lambda''_{321}\lambda''_{231}^*$ and $\lambda''_{221}\lambda''_{331}^*$, have been derived for the first time.

It should be noted that there still are allowed parameters for all relevant \mathcal{L} and \mathcal{B} coupling products if we also add the bounds of C_{B_s} , ϕ_{B_s} , ϕ_s^{NP} and R_s from Unitarity Triangle analysis in Ref. [6]. Comparing with the bounds from ΔM_s , $\phi_s^{J/\psi\phi}$ and $\Delta\Gamma_s$, we find that, after considering to add the bounds of C_{B_s} , ϕ_{B_s} , ϕ_s^{NP} and R_s , the lower limits of moduli of relevant \mathcal{R}_p coupling products will be shrunk and the ranges of the allowed \mathcal{R}_p weak phases will be decreased. More detailed measurements of relevant observables at the Tevatron, the LHC and the B-factories in near future can shrink or reveal the relevant parameter spaces of relevant \mathcal{R}_p couplings.

Acknowledgments

The authors would like to thank Prof. Alexander Lenz and Dr. Guennadi Borissov for helpful comments and suggestions on the manuscript. The work is supported by the National Science Foundation of P.R. China under contract Nos. 11047145 and 11005088.

References

- [1] T. Aaltonen *et al.* [CDF Collaboration], Phys. Rev. Lett. **100**, 161802 (2008) [arXiv:0712.2397 [hep-ex]].
- [2] V. M. Abazov *et al.* [DØ Collaboration], Phys. Rev. Lett. **101**, 241801 (2008) [arXiv:0802.2255 [hep-ex]].
- [3] D. Tonelli [CDF Collaboration], arXiv:0810.3229 [hep-ex].
- [4] V. M. Abazov *et al.* [DØ Collaboration], Phys. Rev. D **82**, 032001 (2010) [arXiv:1005.2757 [hep-ex]].
- [5] CDF/DØ, $\Delta\Gamma$, β_s Combination Working Group, “Combination of DØ and CDF results on $\Delta\Gamma_s$ and the CP-violating phase $\beta_s^{J/\psi\phi}$ ”, Note 5928-CONF, July 22, 2009.
- [6] M. Bona *et al.*, arXiv:0906.0953 [hep-ph].
- [7] A. Lenz and U. Nierste, J. High Energy Physics **0706**, 072 (2007) [arXiv:hep-ph/0612167].
- [8] L. Silvestrini, Nucl. Phys. Proc. Suppl. **185**, 41 (2008).
- [9] M. Bona *et al.* [UTfit Collaboration], PMC Phys. A **3**, 6 (2009) [arXiv:0803.0659 [hep-ph]].
- [10] E. Barberio *et al.* [Heavy Flavor Averaging Group], arXiv:0808.1297 [hep-ex].
- [11] A. Lenz, Nucl. Phys. Proc. Suppl. **177**, 81 (2008) [arXiv:0705.3802 [hep-ph]].
- [12] A. J. Buras, M. V. Carlucci, S. Gori and G. Isidori, arXiv:1005.5310 [hep-ph]; B. A. Dobrescu, P. J. Fox and A. Martin, Phys. Rev. Lett. **105**, 041801 (2010) [arXiv:1005.4238 [hep-ph]].

- [13] C. H. Chen, C. Q. Geng and W. Wang, arXiv:1006.5216 [hep-ph]; C. H. Chen and G. Faisel, arXiv:1005.4582 [hep-ph].
- [14] J. Kubo and A. Lenz, arXiv:1007.0680 [hep-ph]; K. Kawashima, J. Kubo and A. Lenz, Phys. Lett. B **681**, 60 (2009) [arXiv:0907.2302 [hep-ph]].
- [15] O. Eberhardt, A. Lenz and J. Rohrwild, arXiv:1005.3505 [hep-ph]; M. Bobrowski, A. Lenz, J. Riedl and J. Rohrwild, Phys. Rev. D **79**, 113006 (2009) [arXiv:0902.4883 [hep-ph]].
- [16] J. K. Parry, arXiv:1006.5331 [hep-ph]; B. Dutta, Y. Mimura and Y. Santoso, Phys. Rev. D **80**, 095005 (2009) [arXiv:0907.4946 [hep-ph]].
- [17] Q. Chang, X. Q. Li and Y. D. Yang, J. High Energy Physics **1002**, 082 (2010) [arXiv:0907.4408 [hep-ph]]; N. G. Deshpande, X. G. He and G. Valencia, arXiv:1006.1682 [hep-ph].
- [18] C. W. Bauer and N. D. Dunn, arXiv:1006.1629 [hep-ph]; A. Dighe, A. Kundu and S. Nandi, Phys. Rev. D **82**, 031502 (2010) [arXiv:1005.4051 [hep-ph]].
- [19] Y. Bai and A. E. Nelson, arXiv:1007.0596 [hep-ph]; D. Choudhury and D. K. Ghosh, arXiv:1006.2171 [hep-ph]; S. F. King, arXiv:1006.5895 [hep-ph].
- [20] S. Weinberg, Phys. Rev. D **26**, 287 (1982).
- [21] N. Sakai and T. Yanagida, Nucl. Phys. B **197**, 533 (1982); C. Aulakh and R. Mohapatra, Phys. Lett. B **119**, 136 (1982).
- [22] S. Nandi and J. P. Saha, Phys. Rev. D **74**, 095007 (2006) [arXiv:hep-ph/0608341].
- [23] J. P. Saha and A. Kundu, Phys. Rev. D **69**, 016004 (2004) [arXiv:hep-ph/0307259].
- [24] A. Kundu and J. P. Saha, Phys. Rev. D **70**, 096002 (2004) [arXiv:hep-ph/0403154].
- [25] G. Bhattacharyya and A. Raychaudhuri, Phys. Rev. D **57**, 3837 (1998) [arXiv:hep-ph/9712245].
- [26] B. de Carlos and P. L. White, Phys. Rev. D **55**, 4222 (1997) [arXiv:hep-ph/9609443].
- [27] D. Guetta, Phys. Rev. D **58**, 116008 (1998) [arXiv:hep-ph/9805274].

- [28] D. Bećirević *et al.*, Nucl. Phys. B **634**, 105 (2002) [arXiv:hep-ph/0112303].
- [29] D. Bećirević *et al.*, J. High Energy Physics **0204**, 025 (2002) [arXiv:hep-lat/0110091]; D. Bećirević *et al.*, Nucl. Phys. Proc. Suppl. **106**, 385 (2002) [arXiv:hep-lat/0110117].
- [30] G. Buchalla, A. J. Buras and M. E. Lautenbacher, Rev. Mod. Phys. **68**, 1125 (1996) [arXiv:hep-ph/9512380].
- [31] M. Beneke *et al.*, Phys. Lett. B **459**, 631 (1999); A. Lenz, hep-ph/9906317.
- [32] M. Beneke, G. Buchalla and I. Dunietz, Phys. Rev. D **54**, 4419 (1996).
- [33] I. I. Bigi, V. A. Khoze, N. G. Uraltsev and A. I. Sanda, The Question of CP Noninvariance — As Seen Through the Eyes of Neutral Beauty, edited by C. Jarlskog (World Scientific, Singapore, 1989), p.175; J. L. Hewett, T. Takeuchi and S. Thomas, SLAC-PUB-7088 or CERN-TH/96-56; Y. Grossman, Y. Nir, and R. Rattazzi, SLAC-PUB-7379 or CERN-TH-96-368; M. Gronau and D. London, Phys. Rev. D **55**, 2845 (1997).
- [34] Y. Grossman, Phys. Lett. B **380**, 99 (1996).
- [35] S. Baek and P. Ko, Phys. Rev. Lett. **83**, 488 (1999) [arXiv:hep-ph/9812229]; S. Baek and P. Ko, Phys. Lett. B **462**, 95 (1999) [arXiv:hep-ph/9904283]; L. Randall and S. f. Su, Nucl. Phys. B **540**, 37 (1999) [arXiv:hep-ph/9807377].
- [36] Z. Ligeti, M. Papucci and G. Perez, arXiv:hep-ph/0604112; Y. Grossman, Y. Nir and G. Raz, arXiv:hep-ph/0605028.
- [37] C. Amsler *et al.* [Particle Data Group], Phys. Lett. B **667**, 1 (2008) and 2009 partial update for the 2010 edition.
- [38] M. Bona *et al.* [UTfit Collaboration], J. High Energy Physics **0603**, 080 (2006) [hep-ph/0509219].
- [39] A. J. Buras, M. Jamin and P. H. Weisz, Nucl. Phys. B **347**, 491 (1990); J. Urban *et al.*, Nucl. Phys. B **523**, 40 (1998).
- [40] S. Hashimoto, Int. J. Mod. Phys. A **20**, 5133 (2005).

- [41] R. M. Wang, G. R. Lu, E. K. Wang and Y. D. Yang, High Energy Phys. Nucl. Phys. **31**, 332 (2007) [arXiv:hep-ph/0609276].
- [42] Y. D. Yang, R. Wang and G. R. Lu, Phys. Rev. D **73**, 015003 (2006) [arXiv:hep-ph/0509273].
- [43] Y. G. Xu, R. M. Wang and Y. D. Yang, Phys. Rev. D **74**, 114019 (2006) [arXiv:hep-ph/0610338].
- [44] M. Chemtob, Prog. Part. Nucl. Phys. **54**, 71 (2005) [arXiv:hep-ph/0406029].
- [45] D. Chakraverty and D. Choudhury, Phys. Rev. D **63**, 075009 (2001) [arXiv:hep-ph/0008165].